Computational Condensed Matter 35 (2023) e00806

Contents lists available at ScienceDirect

Computational Condensed Matter

journal homepage: www.elsevier.com/locate/cocom

Nearly flat bands and ferromagnetism in the terminated Mn_2C MXene

Victoria V. Kozak [a,b], Natalja A. Fedorova [b], Julia S. Olshevskaya [b], Alena V. Kovaleva [b], Alexander A. Shubin [b], Anton S. Tarasov [a,b], Sergey N. Varnakov [a], Sergei G. Ovchinnikov [a,b], Felix N. Tomilin [a,b,*], Pavel V. Avramov [c,**]

[a] Kirensky Institute of Physics, Federal Research Center KSC SB RAS, Krasnoyarsk, 660036, Russia
[b] Siberian Federal University, Krasnoyarsk, 660041, Russia
[c] Department of Chemistry, College of Natural Sciences, Kyungpook National University, 80 Daehak-ro, Buk-gu, Daegu, 41566, Republic of Korea

ARTICLE INFO

Keywords:
MXene
Nanomaterials
B3LYP
Ferromagnet
Spintronics
2D magnetism
Half metal
Hydroxylated/oxygenated/halogenated MXene

ABSTRACT

Using Density Functional Theory and Periodic Boundary Conditions it is shown that the hydroxylated/oxygenated/halogenated Mn_2C monolayer is a 2D ferromagnetic material with a local *Mn* ions magnetic moment of 2.7μ_B per unit cell. Upon oxygenation the ferromagnetic coupling between Mn ions can be transformed into a superposition of magnetic states. In particular, the intrinsic magnetic moments in the hydroxylated/halogenated Mn_2C monolayer can attain up to 6μ_B per unit cell. It is found that oxygen termination induces flat bands in the band structure, which evidence for the strong electron correlations and could lead to the implementation of exotic quantum phases in 2D crystals and high-temperature superconductivity. Along with the potential of the hydroxylated Mn_2C monolayer characterized by the half-metallicity for application in spintronic devices as a perfect spin injector/detector, this material like other conventional MXenes is promising for the use in energy storage, electromagnetic interference shielding, and sensing.

1. Introduction

During the last 20 years, effective carrier injection, detection and control of spin current was achieved in many spintronics devices based on magnetic tunnel junctions (MTJs) fabricated using both metallic and semiconductor fragments [1–12]. Now attention is paid to the study of quantum, low-dimensional, and topological materials [13–16] successfully used in electronic [17] and optical [18] spintronic devices. A number of low-dimensional materials like graphene [19], nitrides [20], and chalcogenides (-*Hal*) [21] exhibit unique properties prospective for applications in spintronics. Just recently a family of low-dimensional materials is replenished by MXenes [22], i.e., 2D transition metal carbides and nitrides [23]. These compounds can be synthesized by using chemical etching to cleave a hexagonal $M_{n-1}AX_n$ (MAX) layered phases [24], where *M* is the transition metal, *A* is the group-*A* element (e.g., *Si*, *Al*, or *Ga*), and *X* is carbon or nitrogen (*n* can vary from 1 to 4). The energetic and dynamic stability of different kind of MXenes is confirmed by theoretical [25] and experimental results. It was found that semiconducting M_2CO_2-based MXenes with *M* = *Ti*, *Zr*, *Hf* [25] is very promising for thermoelectric applications, whereas M_2CO_2 MXenes with M = *Cr*, *Mn* display distinctive metallic conductivity [25].

Although many 2D compounds are successfully synthesized, the number of ferro- (FM), ferri- and antiferromagnetic (AFM) species is still severely limited [26,27]. Potentially, such 2D lattices can demonstrate low-dimensional magnetism. In combination with other quantum and topological materials they can be used to design prospective heterostructures for novel spin- and quantum-related applications. To date, few FM and AFM compounds of MAX phase family are predicted [28,29] and synthesized, namely the bulk rare-earth *i*-MAX phases ($Mo_{2/3}Re_{1/3})_2AlC$ [30], Mn_2GaC [31,32], and (*Mn*, *Cr*)$_2$*GaC* [33,34] thin films with AFM ordering. The synthesis of FM or AFM MXenes is still an urgent task. Most predicted magnetic MXenes contain 3*d* elements (e.g., *Cr*, *Mn*, *Fe*, *Co*, or *Ni* Transitional Metal (TM) elements) [35–37]. However, even TM-based MAX phases are difficult to synthesize. A distinctive feature of MXenes is the possibility of modifying their properties by functionalization of the surfaces by = *O*, *–OH*, *–Cl*, or *–F* functional groups formed after removal of an element *A* [38,39], which allows one to obtain the desired transport, sensor, magnetic, and other properties [40]. In this regard, the *Mn*-containing magnetic MAX phases and MXenes seem to be the most realistic and promising low-dimensional compounds to be

* Corresponding author. Kirensky Institute of Physics, Federal Research Center KSC SB RAS, Krasnoyarsk, 660036, Russia.
** Corresponding author.
E-mail addresses: felixnt@gmail.com (F.N. Tomilin), paul.veniaminovich@knu.ac.kr (P.V. Avramov).

https://doi.org/10.1016/j.cocom.2023.e00806
Received 22 December 2022; Received in revised form 27 February 2023; Accepted 8 April 2023
Available online 15 April 2023
2352-2143/© 2023 Elsevier B.V. All rights reserved.

synthesized and studied using both experimental and theoretical techniques.

In recent years a number of new methods for MAX phase delamination were proposed [38]. The resent and probably the most promising are (*i*) Lewis acid molten salt etching, which can be used to replace elements that are poorly etched in the parent MAX phase [41], and (*ii*) Ionic liquid-based synthesis based on organic components contained fluorine [42]. In a recent paper by the Rosen group [43] theoretically predicted chemical exfoliation method is proposed to obtain low-dimensional MXenes. A novel insight and development of the production technologies of low-dimensional MXenes with advanced magnetic and spin properties is of fundamental importance for future spin-related applications.

In this work, several ways to modify atomic and electronic structure of 2D Mn_2C monolayers were studied using Density Functional Theory (DFT) within Periodic Boundary Conditions (PBC). It was found that termination of Mn_2C monolayer by *–O* functional groups induces flat bands in the vicinity of the Fermi level, which could be a main sign of strong electron correlations and could cause an implementation of exotic quantum phases and high-temperature superconductivity [44] whereas termination by *-Hal* groups ensures the highest magnetic moments (up to 6 μ_B) per unit cell. The - *OH*-group passivation stabilizes 2D MXene surface and ensures a total magnetic moment of 4.27 μ_B per unit cell and the spin FM ordering. Proposed 2D magnetic phases perspective for FM spintronic devices [45] could be synthesized using either Mn_2GaC or Mn_2AlC compounds as precursors by etching of gallium or aluminum ions from the lattices by hydrofluoric (*HF*) acid with subsequent termination in H_2O.

2. Computational details

To simulate different *Mn*-based MXene phases, carbon was chosen as an element *X* and aluminum was taken as an element *A*, since it is rather easy to etch them from parent MAX phases [46]. Manganese was chosen as an element *M* because of (*i*) a lack of publications devoted to *Mn*-containing phases; (*ii*) its unique magnetic properties in +2 oxidation state; and (*iii*) the possibility to obtain a *Mn*-containing phases by substitution of *Mn* by *Cr*, since *Cr*-containing phases were synthesized experimentally [47–49]. In this regard, it is necessary to note that *Cr* and *Mn* ions have similar radii equal to 0.615 and 0.602 Å, respectively [50]. For the sake of comparison, parent 2D Mn_2AlC MAX phase was initially studied using electronic structure calculations. All lattices display perfect symmetry perpendicular *c* direction, so they do satisfy mandatory requirements of Topology Conservation Theorem [51–54] and PBC can be used to study atomic and electronic structure of all considered phases.

The Density Functional Theory within Periodic Boundary Conditions was employed for electronic structure calculations of crystalline structure and electronic properties of MAX and MXene phases using CRYSTAL 17 code [55]. The DFT B3LYP potential [56] combined with pob-DZVP-rev2 basis set [57] was used to calculate atomic and electronic structure of Mn_2AlC MAX phase. The DFT Perdew-Burke-Ernzerhof (PBE) functional [58] combined with pob-DZVP-rev2 basis set was used to calculate *Mn*-, *C*-, and *O*- based MXene phases. Since the convergence for *H* in this basis turned out to be poor, the 3–1p1G_gatti_1994 basis set [59] was chosen. The cutoff limits in estimating the Coulomb and exchange integrals that arise in the self-consistent field (SCF) equations for periodic systems were set at 10^{-7} a.u. for the Coulomb overlap, 10^{-7} a.u. Coulomb penetration, 10^{-7} a.u. exchange overlap, 10^{-7} a.u. exchange pseudo-overlap in direct space, and 10^{-14} a.u. exchange pseudo-overlap in the reciprocal space. The condition for SCF convergence was set to be 10^{-6} a.u. from the total energy difference between two successive iterative cycles [55]. The shrinking factors for the Pack–Monkhorst [60] and Gilat grids [61] had the same values (8). The atomic coordinate gradients were estimated analytically. The equilibrium structure was determined using the quasi-Newton approach with the Broyden–Fletcher–Goldfarb–Shanno algorithm according to the Hessian matrix update scheme [62]. The total spin magnetic moment per unit cell was preset maximum possible and, after optimization, took its equilibrium value for each lattice. To avoid artificial interactions between mirror partners of 2D lattices, a vacuum gap of 500 Å in *c* direction was introduced for all PBC calculations.

3. Results and discussion

The crystalline structure of Mn_2AlC MAX phase is presented in Fig. 1a. According to the literature data, the Mn_2AlC MAX phase has $P6_3/mmc$ symmetry with three nonequivalent atoms, namely *Mn*, *Al*, and *C* and *a* and *c* translation vectors and $\alpha = \beta = 90^\circ$ and $\gamma = 120^\circ$ angles [63]. Since there is no inversion center in the unit cell, one can expect spin-polarized states in the MAX phases. The DFT PBE/pob-DZVP-rev2 optimization returned $a = 2.87$ Å and $c = 12.44$ Å. The Mulliken spatial charges of *Mn*, *Al* and *C* ions equal to $Z_{Mn} = 0.18\ e^-$, $Z_{Al} = -0.41\ e^-$, and $Z_C = -0.96\ e^-$, respectively were determined with *Mn–C* and *Mn–Al* distances equal to 1.97 Å and 2.63 Å, respectively. Based on PBE-optimized structure, the B3LYP functional optimization using the same symmetry was carried out. The DFT B3LYP/pob-DZVP-rev2 returned optimized *a* and *c* parameters equal to 2.96 and 12.89 Å, respectively, with partial atomic charges $Z_{Mn} = 0.29\ e^-$, $Z_{Al} = -0.44\ e^-$, and $Z_C = -0.13\ e^-$ and *Mn–C*, *Mn–Al*, and *Mn–Mn* distances equal to 2.03 Å, 2.72 Å, 2.96 Å in the same layer, and 2.80 Å in different layers, respectively. The lattice parameters for PBE and B3LYP potentials are close to each other with less than 4% difference. The difference between magnetic moments per cell (PBE = 7.38 μ_B; B3LYP = 11.42 μ_B, Table S1 of Supplementary Information Section (SI) calculated at PBE and B3LYP levels of theory attained 35%, while the difference between the estimated magnetic moments localized at Manganese ions (PBE = 0.18 e^-; B3LYP = 0.29 e^-, Tables S1 and SI) and Mulliken atomic charges approaches to 38%. This means that the electron correlations affect the electronic and spin properties of the lattices and the hybrid functionals are therefore preferred to study structure and properties of MAX and MXene phases.

The partial electronic densities of states (p-DOS, Fig. 1b) in the vicinity of the Fermi level unequivocally demonstrate spin-polarized metallic state of Mn_2AlC MAX phase, mostly determined by partial *Mn* and *Al* partial contributions, which could be promising for spintronics. The band structure (Fig. 1c) coincides well with the results published earlier [64]. The band structure showed that 2D Mn_2AlC MAX phase crystal exhibits the metal-type behavior in the basal plane with numerous bands crossing the Fermi level. Different densities of spin-up (α) and spin-down (β) electrons at the top of the valence band and in the conducting region of the Mn_2AlC structure directly indicate the spin polarization of the carriers.

To calculate the magnetic properties, spin-polarized calculations for a cell consisting of 8 atoms (4 *Mn*, 2 Al, and 2 *C*) were performed for P1 symmetry with the directions of the magnetic moments at *Mn* ions alternate along *c* direction. For convenience, the energy of the magnetic states of all calculations was estimated relative to the ferromagnetic state, since any state can be energetically advantageous for different variants of crystal structures. The maximum magnetic moment was set initially to *Mn* and acquired an equilibrium value during the optimization. The possible magnetic states of Mn_2AlC MAX phase are presented in Fig. 1 of Supplementary Information Section.

According to the data given in Table 1, AFM-5 state is energetically favorable for 2D Mn_2AlC lattice with relative energy in respect to FM state equal to −12.5 kJ/mol. A slight energy differences between different magnetic states may lead to their mixture. The lattice parameters vary insignificantly (less than 1%) upon variation in the magnetic states (Tables S2 and SI).

The MXene Mn_2C lattices [65] were calculated by B3LYP/pob-DZVP-rev2 approach using P1 space symmetry group (Fig. 2, Table 2). For 2D Mn_2C, the PBE optimization procedure returned

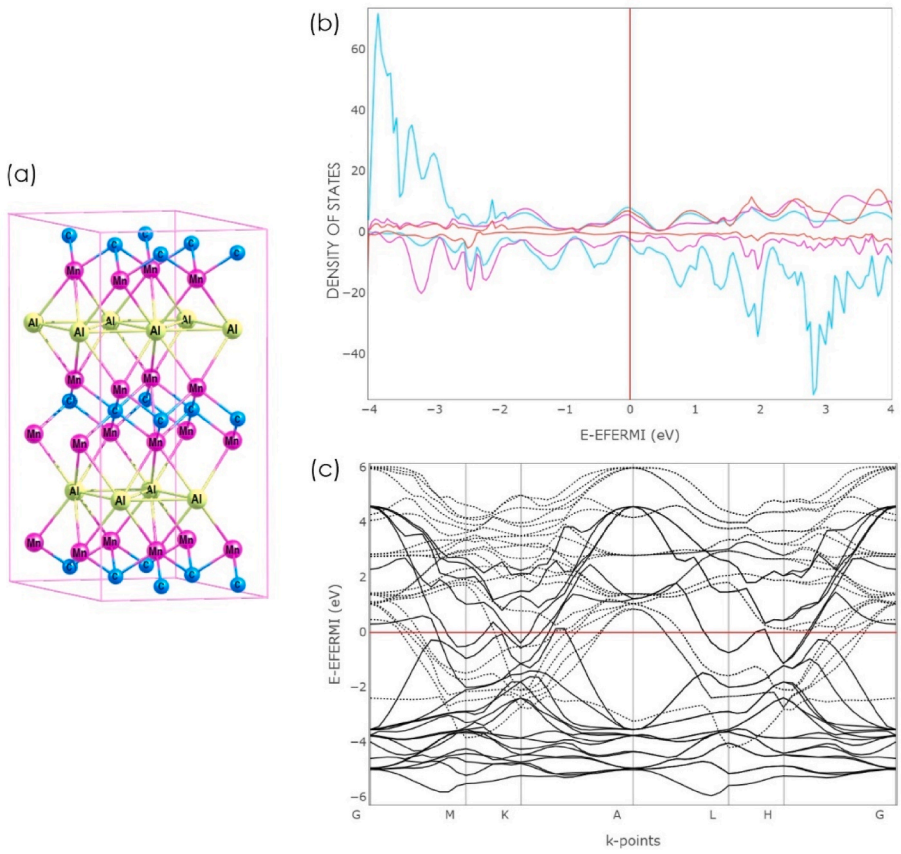

Fig. 1. Crystalline structure, partial density of states and band structure of Mn_2AlC MAX phase calculated at B3LYP/pob-DZVP-rev2 level of theory. (a) Crystalline lattice of the MAX phase with $a = b = 2.96$ Å, and $c = 12.89$ Å parameters. (b) Partial electron density of states (p-DOS) of Mn_2AlC. The red vertical line shows the position of the Fermi level. The blue lines correspond to *Mn* p-DOSes, purple lines represent *Al* p-DOSes, and red lines represent *C* p-DOSes. (c) Band structure of Mn_2AlC MAX phase. The red line marks the Fermi level position. The solid line shows α electrons bands and the dotted line represents the β ones. (For interpretation of the references to color in this figure legend, the reader is referred to the Web version of this article.)

Table 1
Mn_2AlC magnetic moments localized at *Mn* ions.

	FM[a]	AFM-1	AFM-2	AFM-3	AFM-4	AFM-5
Relative energy (kJ/mol)	0[a]	6.91	6.72	34.37	44.78	−12.5
Magnetic moments, μ_B						
Per unit cell	11.43	5.33	5.36	0.38	0.47	0.00
Mn ion (1)[b]	3.37	3.26	3.07	3.26	3.32	3.37
Mn ion (2)	3.37	3.05	3.26	3.41	−3.07	−3.37
Mn ion (3)	3.37	3.28	−3.18	−3.25	−3.06	3.37
Mn ion (4)	3.37	−3.19	3.29	−2.98	3.31	−3.37

[a] The relative FM energy is taken for zero.
[b] Numbering is according to Fig. S1.

$a = b = 2.56$ Å and $\alpha = \beta = 90°$, $\gamma = 120°$ unit cell parameters with $c =$ 500 Å vacuum interval between periodic images.

Pristine hexagonal Mn_2C monolayer presented in the center of Fig. 2 is formed by three atomic *Mn–C–Mn* layers located one above another (see Fig. 2) with *Mn–C* interatomic distances equal to 1.94 Å. All other lattices were formed by passivation of parent Mn_2C monolayer by *F*, *Cl*, *-OH* and *= O* groups from both sides which satisfies mandatory requirements of Topology Conservation Theorem [42]. The *Mn–C* interfragment spacings are equal to 1.68 Å, 1.67 Å 1.63 Å, and 1.62 Å for Mn_2CO_2, $Mn_2C(OH)_2$, Mn_2CF_2, and Mn_2CCl_2, respectively. The occurrence of an oxygen layer in the Mn_2CO_2 structure leads to a strong 13% increase of *a, b* unit cell parameters and slight (0.3%) change of the γ angle. When the hydroxyl group is attached, the parameters *a* and *b* increase by 11% and the angle γ changes slightly within one degree.

The MXenes structural data, band structures and electronic densities of states are presented in Fig. 3 and Table 2 for both α and β spins. All MXenes reveal strongly polarized metallic states since the Fermi level in all the band structures crosses the allowed bands (Fig. 3, left) with large electron density (Fig. 3, right). The 2D Mn_2CO_2 band structure is distinguished from the rest 2D lattices due to the presence of flat exotic bands. Unlike typical quadratic dispersion band and opposite to linear dispersion band, formed by massless Dirac fermions, flat bands carry infinitely heavy fermions, which is very indicative of the strong electron correlations in and manifests itself in other oxide materials, for example, cuprates [66] and cobaltite's [67]. In strongly correlated 2D lattices one can expect the high-temperature superconductivity or other quantum-related electronic transport phenomena, e.g., the fractional quantum Hall effect [68].

The inversion form of the electron densities of states of the Mn_2C, Mn_2CF_2, and Mn_2CCl_2 structures points out the spin polarization of the carriers, which suggests their applicability in spintronics. As can be seen from the data given in Table 2, oxygen atoms which passivate the Mn_2C lattice change the sign of the charge on the *Mn* atom from $-0.03\ e^-$ to $0.40\ e^-$ due to strong oxygen electronegativity which draws off the electron density from the manganese ions. The same can be seen in other 2D lattices saturated by fluorine and chlorine ions.

Recently several *Mn*-based MXenes were synthesized (see, for example [69]) which might display promising magnetic properties. Using PBE and PBE + U PBC Plane Wave electronic structure calculations it was shown that Mn_2C and Mn_2CO_2 display antiferromagnetic semiconducting [70–72] properties. Carbon-based MXenes such as M_2C and M_2CO_2 ($M = Cr, Fe$) [73,74] display a ferromagnetic ground state with Cr_2CF_2 being an antiferromagnetic material [35,73]. MnC_2 may display metallic antiferromagnetic state in contrast to Mn_2CO_2 which could be ferromagnetic [65,75]. The PBE and PBE + U PBC calculations demonstrate a possibility that functionalization of parent Mn_2C by *Cl*, *F* ions and –OH with formation of Mn_2CCl_2, Mn_2CF_2, and $Mn_2C(OH)_2$ [36, 72] may lead to ferromagnetic ground states. Recently it was found that nitrogen-based MXenes ($Mn_2NF_2/Mn_2N(OH)_2/Mn_2NO_2$) demonstrate

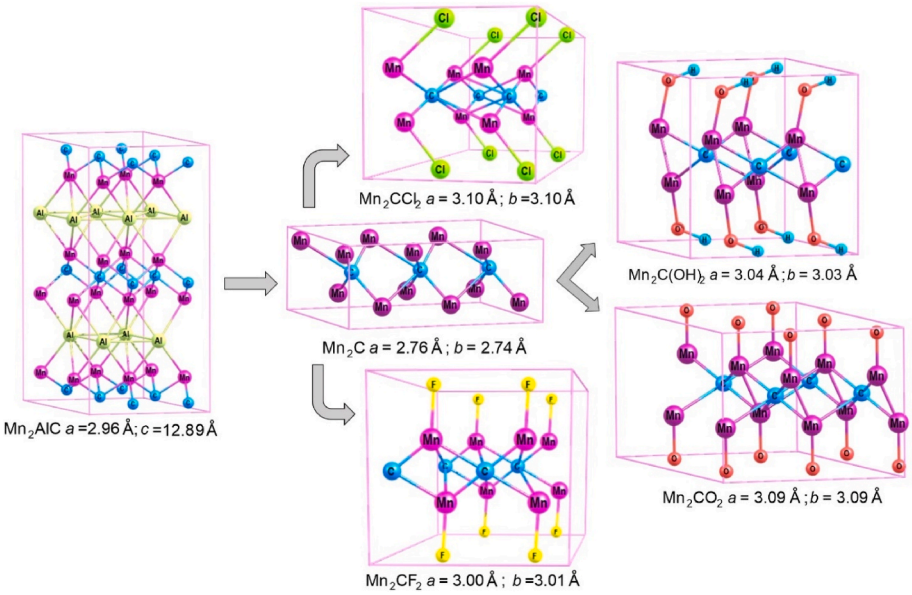

Fig. 2. Schematic of design of the Mn_2C, Mn_2CO_2, $Mn_2C(OH)_2$, Mn_2CF_2, and Mn_2CCl_2 structures using the PBE calculations.

Table 2
Relative energies and magnetic moments of MXene phases.

	Mn_2C			Mn_2CO_2			$Mn_2C(OH)_2$	Mn_2CF_2			Mn_2CCl_2		
	FM	AFM1	AFM2	FM	AFM1	AFM2	FM[b]	FM	AFM1	AFM2	FM	AFM1	AFM2
Relative energy, kJ/mol (the FM energy is taken as zero)													
	0.00	49.10	49.21	0.00	0.17	0.17	0.00	0.00	18.38	14.71	0.00	49.79	49.79
Magnetic moments, μ_B													
Per cell	5.00	0.54	−0.54	0.30	0.00[a]	0.00[a]	4.27	5.63	−0.04	−1.06	4.92	0.21	−0.21
Mn (1)	2.70	−1.18	1.18	0.16	0.00[a]	0.00[a]	2.22	2.86	−2.40	1.75	2.62	−2.48	2.49
Mn (2)	2.69	1.75	−1.75	0.16	0.00[a]	0.00[a]	2.23	2.86	2.36	−2.81	2.61	2.69	−2.69
Mulliken partial charge, e^-													
Mn	−0.03	−0.01	−0.01	0.40	0.40	0.40	0.38	0.39	0.37	0.35	0.36	0.37	0.37
C	0.06	0.02	0.02	−0.14	−0.14	−0.14	−0.13	−0.19	−0.17	−0.16	−0.10	−0.12	−0.12
O	–	–	–	−0.33	−0.34	−0.34	−0.63	–	–	–	–	–	–
F/Cl	–	–	–	–	–	–	–	−0.30	−0.29	−0.28	−0.31	−0.31	−0.31
Lattice parameters (c = 500 Å, α = β = 90°)													
a, Å	2.76	2.67	2.68	3.09	3.09	3.09	3.04	3.00	3.04	3.01	3.10	3.13	3.13
b, Å	2.74	2.68	2.69	3.09	3.09	3.09	3.03	3.01	3.02	2.99	3.10	3.13	3.13
γ, °	119.5	120.8	120.6	119.9	120.0	120.0	121.8	120.1	120.0	119.9	120.0	120.0	120.0

[a] Value less than 0.001.
[b] When the spin state is optimized, the system transitions to a ferromagnetic state.

ferromagnetic ground states [23]. Controversial results obtained using PBE functional stimulate state-of-the-art theoretical consideration of electronic properties and spin states of MXenes using sophisticated hybrid DFT functionals like B3LYP and PBE0 using crystal orbitals basis functions since such approach is suitable for electronic structure calculations of covalent compounds [76].

In order to study the spin states of Mn_2C-based MXenes, namely Mn_2CO_2, $Mn_2C(OH)_2$, Mn_2CF_2, and Mn_2CCl_2, the spin-polarized calculations were performed using P1 unit cells. For each single MXene phase, three possible spin states were determined (Figs. S2 and SI Section). The maximum spin moment was set initially at *Mn* ions and acquired an equilibrium value during the optimization (Table 2). It was shown that for all MXene lattices, the ferromagnetic spin order is energetically favorable. Using manganese spin states one can easily determine oxidative states of *Mn* ions equal to +2 for Mn_2C, Mn_2CF_2, and Mn_2CCl_2 and +3 for $Mn_2C(OH)_2$ and Mn_2CO_2. It is necessary to note that the lattice parameters are not affected by the spin states of the species (Table 2).

At B3LYP/pob-DZVP-rev2 level of theory the highest spin moment localized at *Mn* ions was determined to be equal to 5.63 μ_B for Mn_2CF_2, which makes it very promising for advanced spin-related applications. A dramatic decrease of the spin moments localized at *Mn* ions for 2D Mn_2CO_2 up to 0.30 μ_B per cell with 0.16 μ_B for manganese ions with very small energy difference with the ferromagnetic state of 0.17 kJ/mol, Table 2 in respect to parent 2D Mn_2C is caused by double *Mn═O* chemical bonds localized at the surface. The Mn_2CO_2 could be considered as a very weak ferromagnetic material. The high electronegativity of oxygen ions induces a shift in the electron density with *Mn* ions charges equal to 0.40 e^- for Mn_2CO_2 in contrast to the manganese atomic charge in Mn_2C of −0.03 e^-, with the oxygen ions charge of −0.34 e^-, Table 2. In comparison with O^{2-} ions, the hydroxyl *-OH* groups is much less electronegative with the charge on the *Mn* ion equals to 0.40 e^- for Mn_2CO_2 and 0.38 e^- for $Mn_2C(OH)_2$, Table 2, making $Mn_2C(OH)_2$, a half-metal with non-zero *p*-DOS in α channel (Fig. 3).

4. Conclusions

Using DFT PBC calculations a set of low-dimensional *Mn*-based MXene phases with Halogen (*F*, *Cl*), *-OH*, and *= O* terminating surface functional groups were studied in respect to the parent 2D Mn_2AlC MAX

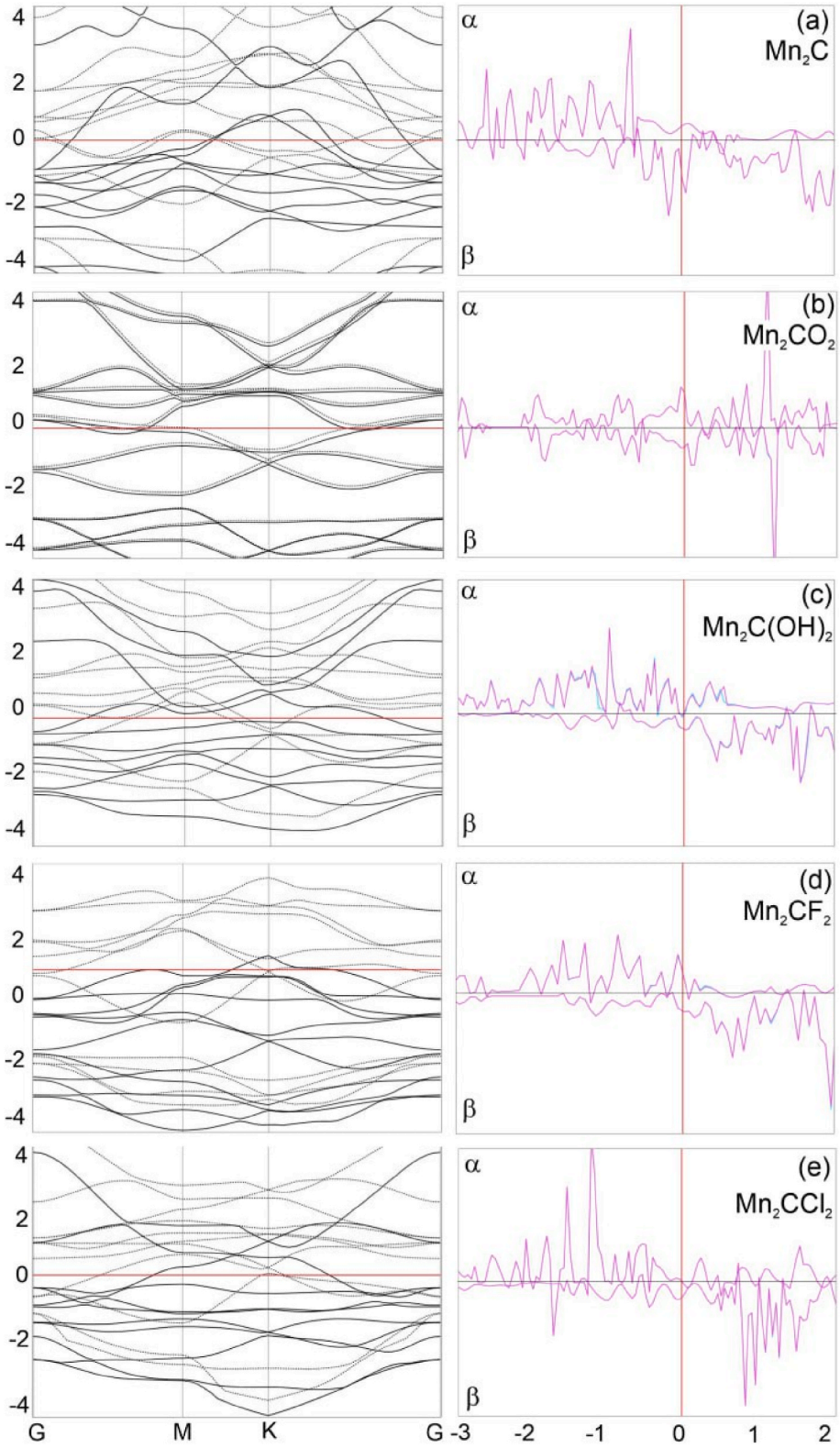

Fig. 3. Band structures (left) and densities of electronic states (right) of 2D MAX and MXene phases. On the left: The red lines in the band structures indicate the Fermi level position. A set of nonequivalent points in the reciprocal space is plotted along the abscissa axis. The solid lines correspond to α electrons and the dotted lines correspond to β electrons. On the right: The red vertical lines in the electron densities of states indicate the Fermi level position. Manganese *p*-DOSes in the upper and lower atomic layers (see Fig. 2and S2) are colored in blue and purple, respectively. The partial DOSes of the other elements are presented in SI Section, Figs. 3S–7 S. (For interpretation of the references to color in this figure legend, the reader is referred to the Web version of this article.)

phase. It was shown that MXene surface termination determines spin and electronic properties of the phases. Mn_2C surface passivation by *F* and *Cl* ions yields the maximum magnetic moments per unit cell up to 5.63 μ_B, while hydroxylation leads to its half-metallicity, whereas oxygenation results in the occurrence of flat bands, which might lead to strongly correlated electronic quantum phases with possible manifestation of quantum-related electron transport phenomena. Wide variation of challenging electronic and spin properties of *Mn*-based MXene phases makes them promising materials for advanced spin- and quantum-related applications. Following DFT simulations, novel low-dimensional MXene phases with advanced electronic and spin properties could be deliberately experimentally developed and synthesized.

Declaration of competing interest

The authors declare that they have no known competing financial interests or personal relationships that could have appeared to influence the work reported in this paper.

Acknowledgments

This study was supported by the Russian Science Foundation, project no. 21-12-00226 and the JCSS Joint Super Computer Center of the Russian Academy of Sciences. P.V.A. acknowledges the National Research Foundation of the Republic of Korea grant NRF 2021R1A2C1010455.

Appendix A. Supplementary data

Supplementary data to this article can be found online at https://doi.org/10.1016/j.cocom.2023.e00806.

References

[1] I. Žutić, J. Fabian, S. Das Sarma, Spintronics: fundamentals and applications, Rev. Mod. Phys. 76 (2004) 323–410, https://doi.org/10.1103/RevModPhys.76.323.
[2] M.N. Baibich, J.M. Broto, A. Fert, F.N. Van Dau, F. Petroff, P. Eitenne, G. Creuzet, A. Friederich, J. Chazelas, Giant magnetoresistance of (001)Fe/(001)Cr magnetic superlattices, Phys. Rev. Lett. 61 (1988) 2472–2475, https://doi.org/10.1103/PhysRevLett.61.2472.
[3] D.C. Ralph, M.D. Stiles, Spin transfer torques, J. Magn. Magn Mater. 320 (2008) 1190–1216, https://doi.org/10.1016/j.jmmm.2007.12.019.
[4] S. Bhatti, R. Sbiaa, A. Hirohata, H. Ohno, S. Fukami, S.N. Piramanayagam, Spintronics based random access memory: a review, Mater. Today 20 (2017) 530–548, https://doi.org/10.1016/j.mattod.2017.07.007.
[5] R. Jansen, Silicon spintronics, Nat. Mater. 11 (2012) 400–408, https://doi.org/10.1038/nmat3293.
[6] D.E. Nikonov, I.A. Young, Overview of beyond-CMOS devices and a uniform methodology for their benchmarking, Proc. IEEE 101 (2013) 2498–2533, https://doi.org/10.1109/JPROC.2013.2252317.
[7] R. Jansen, B.C. Min, S.P. Dash, Oscillatory spin-polarized tunnelling from silicon quantum wells controlled by electric field, Nat. Mater. 9 (2010) 133–138, https://doi.org/10.1038/nmat2605.
[8] K. Hamaya, Y. Fujita, M. Yamada, M. Kawano, S. Yamada, K. Sawano, Spin transport and relaxation in germanium, J. Phys. D Appl. Phys. 51 (2018), 393001, https://doi.org/10.1088/1361-6463/aad542.
[9] S. Gaucher, B. Jenichen, J. Kalt, U. Jahn, A. Trampert, J. Herfort, Growth of Fe3Si/Ge/Fe3Si trilayers on GaAs(001) using solid-phase epitaxy, Appl. Phys. Lett. 110 (2017), https://doi.org/10.1063/1.4977833, 0–5.
[10] A.S. Tarasov, A.V. Lukyanenko, M.V. Rautskii, I.A. Bondarev, D.A. Smolyakov, I. A. Tarasov, I.A. Yakovlev, S.N. Varnakov, S.G. Ovchinnikov, F.A. Baron, N. V. Volkov, Spin-dependent electrical hole extraction from low doped p-Si via the interface states in a Fe3Si/p-Si structure, Semicond. Sci. Technol. 34 (2019), 035024, https://doi.org/10.1088/1361-6641/ab0327.
[11] A.S. Tarasov, I.A. Tarasov, I.A. Yakovlev, M.V. Rautskii, I.A. Bondarev, A. V. Lukyanenko, M.S. Platunov, M.N. Volochaev, D.D. Efimov, A.Y. Goikhman, B. A. Belyaev, F.A. Baron, L.V. Shanidze, M. Farle, S.N. Varnakov, S.G. Ovchinnikov, N.V. Volkov, Asymmetric interfaces in epitaxial off-stoichiometric Fe3+xSi1−x/Ge/Fe3+x Si1−x hybrid structures: effect on magnetic and electric transport properties, Nanomaterials 12 (2022) 1–21, https://doi.org/10.3390/nano12010131.
[12] I.A. Melchakova, T.G. Tenev, N.V. Vitanov, O.N. Tchaikovskaya, L. A. Chernozatonskii, B.I. Yakobson, P.V. Avramov, Extreme structure and spontaneous lift of spin degeneracy in doped perforated bilayer graphenes, Carbon N. Y. 192 (2022) 61–70, https://doi.org/10.1016/j.carbon.2022.02.041.
[13] F. Wu, I. Gutiérrez-Lezama, S.A. López-Paz, M. Gibertini, K. Watanabe, T. Taniguchi, F.O. von Rohr, N. Ubrig, A.F. Morpurgo, Quasi-1D electronic transport in a 2D magnetic semiconductor, Adv. Mater. 34 (2022), 2109759, https://doi.org/10.1002/adma.202109759.
[14] M.M. Otrokov, I.I. Klimovskikh, H. Bentmann, D. Estyunin, A. Zeugner, Z.S. Aliev, S. Gaß, A.U.B. Wolter, A.V. Koroleva, A.M. Shikin, M. Blanco-Rey, M. Hoffmann, I. P. Rusinov, A.Y. Vyazovskaya, S.V. Eremeev, Y.M. Koroteev, V.M. Kuznetsov, F. Freyse, J. Sánchez-Barriga, I.R. Amiraslanov, M.B. Babanly, N.T. Mamedov, N. A. Abdullayev, V.N. Zverev, A. Alfonsov, V. Kataev, B. Büchner, E.F. Schwier, S. Kumar, A. Kimura, L. Petaccia, G. Di Santo, R.C. Vidal, S. Schatz, K. Kißner, M. Ünzelmann, C.H. Min, S. Moser, T.R.F. Peixoto, F. Reinert, A. Ernst, P. M. Echenique, A. Isaeva, E.V. Chulkov, Prediction and observation of an antiferromagnetic topological insulator, Nature 576 (2019) 416–422, https://doi.org/10.1038/s41586-019-1840-9.
[15] L.V. Begunovich, A.V. Kuklin, M.A. Visotin, A.A. Kuzubov, F.N. Tomilin, A. S. Tarasov, Y.G. Mikhalev, P.V. Avramov, Triple VTe2/graphene/VTe2 heterostructures as perspective magnetic tunnel junctions, Appl. Surf. Sci. 510 (2020), 145315, https://doi.org/10.1016/j.apsusc.2020.145315.
[16] B.A. Bernevig, C. Felser, H. Beidenkopf, Progress and prospects in magnetic topological materials, Nature 603 (2022) 41–51, https://doi.org/10.1038/s41586-021-04105-x.
[17] D.R. Klein, D. MacNeill, J.L. Lado, D. Soriano, E. Navarro-Moratalla, K. Watanabe, T. Taniguchi, S. Manni, P. Canfield, J. Fernández-Rossier, P. Jarillo-Herrero, Probing magnetism in 2D van der Waals crystalline insulators via electron tunneling, Science 360 (80) (2018) 1218–1222, https://doi.org/10.1126/science.aar3617.
[18] S. Jiang, L. Li, Z. Wang, K.F. Mak, J. Shan, Controlling magnetism in 2D CrI3 by electrostatic doping, Nat. Nanotechnol. 13 (2018) 549–553, https://doi.org/10.1038/s41565-018-0135-x.
[19] K.S. Novoselov, S.V. Morozov, T.M.G. Mohinddin, L.A. Ponomarenko, D.C. Elias, R. Yang, I.I. Barbolina, P. Blake, T.J. Booth, D. Jiang, J. Giesbers, E.W. Hill, A. K. Geim, Electronic properties of graphene, Phys. Status Solidi Basic Res. 244 (2007) 4106–4111, https://doi.org/10.1002/pssb.200776208.
[20] K. Zhang, Y. Feng, F. Wang, Z. Yang, J. Wang, Two dimensional hexagonal boron nitride (2D-hBN): synthesis, properties and applications, J. Mater. Chem. C 5 (2017) 11992–12022, https://doi.org/10.1039/c7tc04300g.
[21] Y. Shi, H. Li, L.J. Li, Recent advances in controlled synthesis of two-dimensional transition metal dichalcogenides via vapour deposition techniques, Chem. Soc. Rev. 44 (2015) 2744–2756, https://doi.org/10.1039/c4cs00256c.
[22] M. Naguib, O. Mashtalir, J. Carle, V. Presser, J. Lu, L. Hultman, Y. Gogotsi, M. W. Barsoum, Two-dimensional transition metal carbides, ACS Nano 6 (2012) 1322–1331, https://doi.org/10.1021/nn204153h.
[23] H. Kumar, N.C. Frey, L. Dong, B. Anasori, Y. Gogotsi, V.B. Shenoy, Tunable magnetism and transport properties in nitride MXenes, ACS Nano 11 (2017) 7648–7655, https://doi.org/10.1021/ACSNANO.7B02578/ASSET/IMAGES/LARGE/NN-2017-025784_0004.JPEG.
[24] M. Sokol, V. Natu, S. Kota, M.W. Barsoum, On the chemical diversity of the MAX phases, Trends Chem 1 (2019) 210–223, https://doi.org/10.1016/j.trechm.2019.02.016.
[25] A.N. Gandi, H.N. Alshareef, U. Schwingenschlögl, Thermoelectric performance of the MXenes M2CO2 (M = Ti, Zr, or Hf), Chem. Mater. 28 (2016) 1647–1652, https://doi.org/10.1021/ACS.CHEMMATER.5B04257/ASSET/IMAGES/LARGE/CM-2015-042579_0003.JPEG.
[26] M. Gibertini, M. Koperski, A.F. Morpurgo, K.S. Novoselov, Magnetic 2D materials and heterostructures, Nat. Nanotechnol. 14 (2019) 408–419, https://doi.org/10.1038/s41565-019-0438-6.
[27] K.F. Mak, J. Shan, D.C. Ralph, Probing and controlling magnetic states in 2D layered magnetic materials, Nat. Rev. Phys. 1 (2019) 646–661, https://doi.org/10.1038/s42254-019-0110-y.
[28] A.S. Ingason, M. Dahlqvist, J. Rosen, Magnetic MAX phases from theory and experiments; A review, J. Phys. Condens. Matter 28 (2016), https://doi.org/10.1088/0953-8984/28/43/433003.
[29] V.S. Zhandun, N.G. Zamkova, O.N. Draganyuk, A.S. Shinkorenko, U. Wiedwald, S. G. Ovchinnikov, M. Farle, The effect of the composition and pressure on the phase stability and electronic, magnetic, and elastic properties of M2AX (M = Mn, Fe; A = Al, Ga, Si, Ge; X = C, N) phases, Phys. Chem. Chem. Phys. 23 (2021) 26376–26384, https://doi.org/10.1039/d1cp03427h.
[30] Q. Tao, J. Lu, M. Dahlqvist, A. Mockute, S. Calder, A. Petruhins, R. Meshkian, O. Rivin, D. Potashnikov, E.N. Caspi, H. Shaked, A. Hoser, C. Opagiste, R. M. Galera, R. Salikhov, U. Wiedwald, C. Ritter, A.R. Wildes, B. Johansson, L. Hultman, M. Farle, M.W. Barsoum, J. Rosen, Atomically layered and ordered rare-earth i-MAX phases: a new class of magnetic quaternary compounds, Chem. Mater. 31 (2019) 2476–2485, https://doi.org/10.1021/acs.chemmater.8b05298.
[31] I.P. Novoselova, A. Petruhins, U. Wiedwald, Á.S. Ingason, T. Hase, F. Magnus, V. Kapaklis, J. Palisaitis, M. Spasova, M. Farle, J. Rosen, R. Salikhov, Large uniaxial magnetostriction with sign inversion at the first order phase transition in the nanolaminated Mn2GaC MAX phase, Sci. Rep. 8 (2018) 1–11, https://doi.org/10.1038/s41598-018-20903-2.
[32] S. Lyaschenko, O. Maximova, D. Shevtsov, S. Varnakov, I. Tarasov, U. Wiedwald, J. Rosen, S. Ovchinnikov, M. Farle, Optical and magneto-optical properties of epitaxial Mn2GaC MAX phase thin film, J. Magn. Magn Mater. 528 (2021), 167803, https://doi.org/10.1016/j.jmmm.2021.167803.
[33] A. Petruhins, A.S. Ingason, J. Lu, F. Magnus, S. Olafsson, J. Rosen, Synthesis and characterization of magnetic (Cr0.5Mn0.5)2GaC thin films, J. Mater. Sci. 50 (2015) 4495–4502, https://doi.org/10.1007/s10853-015-8999-8.
[34] I.P. Novoselova, A. Petruhins, U. Wiedwald, D. Weller, J. Rosen, M. Farle, R. Salikhov, Long-term stability and thickness dependence of magnetism in thin (Cr0.5 Mn0.5)2GaC MAX phase films, Mater. Res. Lett. 7 (2019) 159–163, https://doi.org/10.1080/21663831.2019.1570980.
[35] J. Yang, S. Zhang, A. Wang, R. Wang, C.K. Wang, G.P. Zhang, L. Chen, High magnetoresistance in ultra-thin two-dimensional Cr-based MXenes, Nanoscale 10 (2018) 19492–19497, https://doi.org/10.1039/c8nr04978e.
[36] E. Balcl, Ü.Ö. Akkuş, S. Berber, High TMR in MXene-based Mn2CF2/Ti2CO2/Mn2CF2 magnetic tunneling junction, ACS Appl. Mater. Interfaces 11 (2019) 3609–3616, https://doi.org/10.1021/acsami.8b20202.
[37] X. Jiang, A.V. Kuklin, A. Baev, Y. Ge, H. Ågren, H. Zhang, P.N. Prasad, Two-dimensional MXenes: from morphological to optical, electric, and magnetic properties and applications, Phys. Rep. 848 (2020) 1–58, https://doi.org/10.1016/j.physrep.2019.12.006.
[38] Y. Wei, P. Zhang, R.A. Soomro, Q. Zhu, B. Xu, Advances in the synthesis of 2D MXenes, Adv. Mater. 33 (2021), 2103148, https://doi.org/10.1002/adma.202103148.
[39] Y.J. Kim, S.J. Kim, D. Seo, Y. Chae, M. Anayee, Y. Lee, Y. Gogotsi, C.W. Ahn, H. T. Jung, Etching mechanism of monoatomic aluminum layers during MXene

synthesis, Chem. Mater. 33 (2021) 6346–6355, https://doi.org/10.1021/acs.chemmater.1c01263.
[40] A.V. Mohammadi, J. Rosen, Y. Gogotsi, The world of two-dimensional carbides and nitrides (MXenes), Science 372 (80) (2021) 1–14, https://doi.org/10.1126/science.abf1581.
[41] M. Li, J. Lu, K. Luo, Y. Li, K. Chang, K. Chen, J. Zhou, J. Rosen, L. Hultman, P. Eklund, P.O.Å. Persson, S. Du, Z. Chai, Z. Huang, Q. Huang, Element replacement approach by reaction with Lewis acidic molten salts to synthesize nanolaminated MAX phases and MXenes, J. Am. Chem. Soc. 141 (2019) 4730–4737, https://doi.org/10.1021/jacs.9b00574.
[42] S. Husmann, Ö. Budak, H. Shim, K. Liang, M. Aslan, A. Kruth, A. Quade, M. Naguib, V. Presser, Ionic liquid-based synthesis of MXene, Chem. Commun. 56 (2020) 11082–11085, https://doi.org/10.1039/D0CC03189E.
[43] J. Björk, J. Halim, J. Zhou, J. Rosen, Predicting chemical exfoliation: fundamental insights into the synthesis of MXenes, npj 2D Mater, Apple 7 (2023), https://doi.org/10.1038/S41699-023-00370-8.
[44] M. Imada, M. Kohno, Superconductivity from flat dispersion designed in doped mott insulators, Phys. Rev. Lett. 84 (2000) 143–146, https://doi.org/10.1103/PhysRevLett.84.143.
[45] V. Baltz, A. Manchon, M. Tsoi, T. Moriyama, T. Ono, Y. Tserkovnyak, Antiferromagnetic spintronics, Rev. Mod. Phys. 90 (2018), 015005, https://doi.org/10.1103/RevModPhys.90.015005.
[46] B. Anasori, M.R. Lukatskaya, Y. Gogotsi, 2D metal carbides and nitrides (MXenes) for energy storage, Nat. Rev. Mater. 2 (2017), https://doi.org/10.1038/natrevmats.2016.98.
[47] B. Shalini Reghunath, D. Davis, K.R. Sunaja Devi, Synthesis and characterization of Cr2AlC MAX phase for photocatalytic applications, Chemosphere 283 (2021), 131281, https://doi.org/10.1016/J.CHEMOSPHERE.2021.131281.
[48] K. Sobolev, A. Pazniak, O. Shylenko, V. Komanicky, A. Provino, P. Manfrinetti, D. Peddis, V. Rodionova, Complex optimization of arc melting synthesis for bulk Cr2AlC MAX-phase, Ceram. Int. 47 (2021) 7745–7752, https://doi.org/10.1016/J.CERAMINT.2020.11.119.
[49] M. Magnuson, M. Mattesini, Magnetic anisotropy in Cr2GeC investigated by X-ray magnetic circular dichroism and ab initio calculations, J. Magn. Magn Mater. 501 (2020), 166470, https://doi.org/10.1016/J.JMMM.2020.166470.
[50] D.C. Ghosh, R. Biswas, Theoretical calculation of absolute radii of atoms and ions. Part 2. The ionic radii, Int. J. Mol. Sci. 4 (2003) 379–407, https://doi.org/10.3390/I4060379, 4 (2003) 379–407.
[51] P. V Avramov, A. Kuklin, Topological and quantum stability of low-dimensional crystalline lattices with multiple nonequivalent sublattices, New J. Phys. 24 (2022), 103015, https://doi.org/10.1088/1367-2630/ac93a9.
[52] A.V. Kuklin, H. Ågren, P.V. Avramov, Structural stability of single-layer PdSe2 with pentagonal puckered morphology and its nanotubes, Phys. Chem. Chem. Phys. 22 (2020) 8289–8295, https://doi.org/10.1039/d0cp00979b.
[53] P. Avramov, V. Demin, M. Luo, C.H. Choi, P.B. Sorokin, B. Yakobson, L. Chernozatonskii, Translation symmetry breakdown in low-dimensional lattices of pentagonal rings, J. Phys. Chem. Lett. 6 (2015) 4525–4531, https://doi.org/10.1021/acs.jpclett.5b02309.
[54] P.V. Avramov, D.G. Fedorov, P.B. Sorokin, S. Sakai, S. Entani, M. Ohtomo, Y. Matsumoto, H. Naramoto, Intrinsic edge asymmetry in narrow zigzag hexagonal heteroatomic nanoribbons causes their subtle uniform curvature, J. Phys. Chem. Lett. 3 (2012) 2003–2008, https://doi.org/10.1021/jz300625t.
[55] R. Dovesi, V.R. Saunders, C. Roetti, R. Orlando, C.M. Zicovich-Wilson, F. Pascale, B. Civalleri, K. Doll, N.M. Harrison, I.J. Bush, P. D'Arco, M. Llunel, M. Causà, Y. Noël, L. Maschio, A. Erba, M. Rérat, S. Casassa, CRYSTAL17 User's Manual, 2018. http://tutorials.crystalsolutions.eu/.
[56] A.D. Becke, Density-functional thermochemistry. III. The role of exact exchange, J. Chem. Phys. 98 (1993) 5648–5652, https://doi.org/10.1063/1.464913.
[57] D. Vilela Oliveira, J. Laun, M.F. Peintinger, T. Bredow, BSSE-correction scheme for consistent Gaussian basis sets of double- and triple-zeta valence with polarization quality for solid-state calculations, J. Comput. Chem. 40 (2019) 2364–2376, https://doi.org/10.1002/jcc.26013.
[58] J.P. Perdew, K. Burke, M. Ernzerhof, Generalized gradient approximation made simple, Phys. Rev. Lett. 77 (1996) 3865–3868, https://doi.org/10.1103/PhysRevLett.77.3865.
[59] C. Gatti, V.R. Saunders, C. Roetti, Crystal field effects on the topological properties of the electron density in molecular crystals: the case of urea, J. Chem. Phys. 101 (1994) 10686–10696, https://doi.org/10.1063/1.467882.
[60] H.J. Monkhorst, J.D. Pack, Special Points for Brillonin-Zone Integrations, 1976, https://doi.org/10.1103/PhysRevB.13.5188. NUMBER. 13.
[61] G. Gilat, L.J. Raubenheimert, Accurate Numerical Method. for Calculating Frequency-Distribution Functions in Solids*, (б. д.). https://doi.org/10.1103/PhysRev.144.390.
[62] D.R. Civalleri, B. D'Arco Ph, R. Orlando, V.R. Saunders, Hartree - Fock Geometry Optimisation of Periodic Systems with the CRYSTAL Code, 2001, p. 348, https://doi.org/10.1016/S0009-2614(01)01081-8.
[63] A. Thore, M. Dahlqvist, B. Alling, J. Rosén, First-principles calculations of the electronic, vibrational, and elastic properties of the magnetic laminate Mn2GaC, J. Appl. Phys. 116 (2014), https://doi.org/10.1063/1.4894411.
[64] W. Setyawan, S. Curtarolo, High-throughput electronic band structure calculations: challenges and tools, Comput. Mater. Sci. 49 (2010) 299–312, https://doi.org/10.1016/j.commatsci.2010.05.010.
[65] X. Zhang, T. He, W. Meng, L. Jin, Y. Li, X. Dai, G. Liu, Mn2C monolayer: hydrogenation/oxygenation-induced strong ferromagnetism and potential applications, J. Phys. Chem. C 123 (2019) 16388–16392, https://doi.org/10.1021/acs.jpcc.9b04445.
[66] M.M. Korshunov, S.G. Ovchinnikov, E.I. Shneyder, V.A. Gavrichkov, Y.S. Orlov, I. A. Nekrasov, Z.V. Pchelkina, Cuprates, manganites and cobaltites: multielectron approach to the band structure, Mod. Phys. Lett. B 26 (2012) 1–25, https://doi.org/10.1142/S0217984912300165.
[67] Y.S. Orlov, S.V. Nikolaev, V.A. Dudnikov, S.G. Ovchinnikov, Forming a dielectric exciton phase in strongly correlated systems with spin crossover, Phys. Rev. B 104 (2021) 1–10, https://doi.org/10.1103/PhysRevB.104.195103.
[68] T. Neupert, L. Santos, C. Chamon, C. Mudry, Fractional quantum hall states at zero magnetic field, Phys. Rev. Lett. 106 (2011), 236804, https://doi.org/10.1103/PhysRevLett.106.236804.
[69] T.B. Limbu, S. Kumari, Z. Wang, C. Dhital, Q. Li, Y. Tang, F. Yan, Ingeniously enhanced ferromagnetism in chemically-reduced 2D Ti3C2TX MXene, Mater. Chem. Phys. 285 (2022), 126155, https://doi.org/10.1016/J.MATCHEMPHYS.2022.126155.
[70] Z. Chen, S. Huang, X. Yuan, X. Gan, N. Zhou, A comparative study of M2CS2 and M2CO2 MXenes as anode materials for lithium ion batteries, Appl. Surf. Sci. 544 (2021), https://doi.org/10.1016/J.APSUSC.2020.148861.
[71] Y. Zhou, X. Zu, Mn2C sheet as an electrode material for lithium-ion battery: a first-principles prediction, Electrochim. Acta 235 (2017) 167–174, https://doi.org/10.1016/J.ELECTACTA.2017.03.111.
[72] J. He, P. Lyu, P. Nachtigall, New two-dimensional Mn-based MXenes with room-temperature ferromagnetism and half-metallicity, J. Mater. Chem. C 4 (2016) 11143–11149, https://doi.org/10.1039/C6TC03917K.
[73] C. Si, J. Zhou, Z. Sun, Half-metallic ferromagnetism and surface functionalization-induced metal-insulator transition in graphene-like two-dimensional Cr2C crystals, ACS Appl. Mater. Interfaces 7 (2015) 17510–17515, https://doi.org/10.1021/ACSAMI.5B05401.
[74] H. Hadipour, Y. Yekta, Ab initio study of the effective Coulomb interactions and Stoner ferromagnetism in M2 C and M2CO2 MX- enes (M= Sc, Ti, V, Cr, Fe, Zr, Nb, Mo, Hf, Ta) AB INITIO STUDY of the EFFECTIVE … H. HADIPOUR and Y. YEKTA, Phys. Rev. B 100 (2019) 1–12, https://doi.org/10.1103/PhysRevB.100.195118.
[75] L. Hu, X. Wu, J. Yang, Mn2C monolayer: a 2D antiferromagnetic metal with high Néel temperature and large spin-orbit coupling, Nanoscale 8 (2016) 12939–12945, https://doi.org/10.1039/c6nr02417c.
[76] P.V. Avramov, K.N. Kudin, G.E. Scuseria, Single wall carbon nanotubes density of states: comparison of experiment and theory, Chem. Phys. Lett. 370 (2003) 597–601, https://doi.org/10.1016/S0009-2614(03)00113-1.